SPATIAL DISTRIBUTION OF TENSILE PROPERTIES IN DIRECT CHILL CAST EN AW-5083 ALLOY INGOTS

Natalija Dolić[1*] – Franjo Kozina[1] – Ivana Bunjan[2]

[1]Department of Process Metallurgy, Faculty of Metallurgy, University of Zagreb, Aleja narodnih heroja 3, Sisak, Croatia
[2]Končar Power Transformers, Ltd., Josipa Mokrovića 12, 10090 Zagreb, Croatia

ARTICLE INFO

***Article history*:**
Received: 22. 3. 2026.
Received in revised form: 22. 4. 2026.
Accepted: 22. 4. 2026.

Keywords:
EN AW-5083 aluminium alloy
Direct Chill casting
Tensile properties
Spatial distribution
Microstructure
Analysis of variance

DOI: 10.30765/er.3259

Abstract:

The spatial distribution of tensile properties in EN AW-5083 aluminium alloy ingots produced by the semi-continuous Direct Chill (DC) casting process was investigated under industrial conditions. Tensile tests were performed on samples taken from predefined positions within the ingot cross-section according to a Latin square experimental design, enabling systematic evaluation of spatial variability. The analysed parameters included yield strength ($R_{p0.2}$) and elongation (A_{50}), while the microstructural parameter expressed as the number of grains per unit area (NA) was adopted from previously reported measurements. The results show that both tensile properties vary across the ingot cross-section, with yield strength ranging from 171.5 MPa to 221.0 MPa and elongation from 14% to 27%. Despite these local variations, the average values for the front and rear sections of the ingots were very similar, indicating relatively uniform mechanical behaviour along the casting direction. Statistical analysis based on ANOVA revealed that spatial position within the ingot cross-section has a stronger and more consistent influence on elongation than on yield strength. Slice width showed a statistically significant effect on yield strength in the front section, while both slice height and slice width significantly affected elongation. The observed behaviour is associated with non-uniform solidification conditions typical of DC casting, where variations in cooling rate lead to differences in microstructure. Overall, the investigated ingots exhibit a satisfactory level of structural and mechanical homogeneity, and the results contribute to a better understanding of the relationship between solidification conditions, microstructure, and tensile behaviour.

1 Introduction

Al–Mg alloys are among the non-heat-treatable aluminium alloys, characterised by a favourable combination of mechanical strength, ductility, corrosion resistance, and weldability [1] - [3]. Due to these properties, 5xxx series alloys are widely used in marine structures, transportation systems, storage tanks, and other structural applications requiring a high strength-to-weight ratio and reliable corrosion performance [1], [4], [5]. In these alloys, magnesium (Mg) is the principal alloying element and provides solid-solution strengthening, playing a key role in determining the overall mechanical and corrosion behaviour of the 5xxx series [1], [6]. Among them, EN AW-5083 is one of the most widely used alloys in shipbuilding and structural engineering due to its balanced property profile [1]. In non-heat-treatable aluminium alloys, mechanical properties are primarily determined by solid-solution strengthening and the microstructural characteristics developed during solidification and subsequent thermomechanical processing [6], [7]. Grain size, grain

* Corresponding author
E-mail address:ndolic@simet.unizg.hr

morphology, and the distribution of intermetallic phases therefore play important roles in determining the strength and ductility of these alloys, while crystallographic texture developed during processing may further influence their mechanical behaviour [1], [6], [8]. Large aluminium slabs and billets intended for subsequent rolling or extrusion are most commonly produced using the Direct Chill (DC) casting process, which is the dominant industrial technology for producing wrought aluminium alloy ingots [9] - [11]. During DC casting, molten metal is poured into a water-cooled mould where primary solidification occurs. Further solidification of the partially solidified ingot is achieved by intensive secondary water cooling [12]. Due to the solidification conditions characteristic of the DC casting process, heat extraction occurs mainly through the mould walls and the secondary cooling zone [9], [10]. Consequently, significant thermal gradients develop across the ingot cross-section, leading to non-uniform solidification conditions within the ingot [10], [13] - [15].

The cooling rate is considerably higher near the ingot surface than in the central regions, resulting in spatial variations in dendritic structure, grain size, and chemical segregation across the ingot cross-section [9], [10], [16]. Such microstructural heterogeneity may subsequently influence the mechanical properties of the alloy. The microstructure of DC-cast aluminium alloys is strongly influenced by casting parameters such as melt temperature, casting speed, cooling intensity, and grain-refinement practices [15], [17]. Grain refinement, typically achieved by adding Al–Ti–B master alloys, promotes the formation of fine equiaxed grains and enhances the structural homogeneity and mechanical properties of aluminium castings [17] - [20]. However, even with the use of grain refiners, differences in local cooling conditions within large DC-cast ingots may still cause spatial variations in grain structure. As nucleation and grain growth during solidification are strongly controlled by local cooling rates and thermal gradients, variations in heat extraction across the ingot cross-section inevitably result in spatial differences in grain structure and other microstructural characteristics [9], [15], [20]. Previous investigations of EN AW-5083 alloy ingots produced by the DC casting process have shown that both microstructural characteristics and mechanical properties vary the sampling position within the ingot cross-section [21]. Statistical evaluation of tensile properties measured at different sampling positions revealed spatial variability in mechanical behaviour, attributable to differences in solidification conditions within the ingot [21]. Earlier microstructural studies of the same alloy system also showed pronounced variations in the number of grains per unit area (N_A) across the ingot cross-section, resulting from differences in local cooling conditions during solidification [22]. Higher cooling rates near the ingot surface generally lead to higher N_A values than those in the central regions of the ingot, reflecting the influence of local heat extraction and solidification dynamics during DC casting [22].

As grain size and grain structure strongly influence the mechanical behaviour of aluminium alloys, variations in N_A may significantly affect tensile properties, including yield strength and elongation. Finer-grain structures generally increase strength and may improve ductility due to more homogeneous plastic deformation [1], [6]. More recently, correlations between the number of grains per unit area and ultimate tensile strength in EN AW-5083 DC-cast ingots were analysed using a statistical approach based on the Latin square experimental design [23]. These results confirmed that microstructural heterogeneity associated with casting conditions may directly influence the spatial distribution of mechanical properties within industrial DC-cast ingots. Together, these studies established a systematic experimental framework for evaluating the structural and mechanical homogeneity of DC-cast EN AW-5083 alloy ingots based on statistically defined sampling positions and correlations between microstructural parameters and tensile properties. Therefore, the aim of the present study is to analyse the spatial distribution of yield strength ($R_{p0.2}$) and elongation (A_{50}) in industrially produced DC-cast EN AW-5083 alloy ingots. The influence of melt charge and sampling position within the ingot cross-section was evaluated using a structured Latin square experimental design and analysis of variance (ANOVA). The working hypothesis of this research is that local solidification conditions during the DC casting process lead to spatial variations in the number of grains per unit area (N_A) across the ingot cross-section, which in turn influence the spatial distribution of mechanical properties such as yield strength ($R_{p0.2}$) and elongation (A_{50}).

2 Experimental investigation

2.1 Industrial DC Casting of EN AW-5083 alloy ingots

EN AW-5083 aluminium alloy ingots were produced under industrial conditions using a semi-continuous DC casting process on a Pechiney ingot casting line. The chemical composition of the EN AW-5083 alloy melts (charges 3157, 3158, 3159, 3160, 3162, and 3163) was determined by optical emission spectroscopy (OES) using samples collected during casting, with ingot lengths of approximately 500 mm. The chemical

composition complied with the requirements specified in *EN 573-3* [24], and the detailed compositions of the investigated charges are presented in Table 1 [23].

Table 1. Chemical composition of the investigated EN AW-5083 alloy charges, wt%.

Charge	Si	Fe	Cu	Mn	Mg	Cr	Zn	Ti	Be
3157	0.160	0.420	0.01	0.450	4.410	0.100	0.004	0.024	0.003
3158	0.140	0.350	0.01	0.445	4.325	0.070	0.004	0.021	0.003
3159	0.150	0.385	0.01	0.470	4.175	0.090	0.005	0.025	0.003
3160	0.160	0.430	0.01	0.440	4.390	0.080	0.005	0.024	0.004
3162	0.160	0.350	0.01	0.425	4.350	0.100	0.004	0.022	0.003
3163	0.175	0.375	0.01	0.435	4.490	0.090	0.004	0.023	0.004

Primary electrolytic aluminium and secondary aluminium in the form of process scrap (EN AW-1050, EN AW-5754, EN AW-5049, and EN AW-5083 alloys) were used as raw materials. The charge was melted in gas-fired melting furnaces at temperatures ranging from 760–850 °C. To achieve the required chemical composition, alloying was performed by adding pure metals and master alloys (AlMn, AlCr, and AlMg). To reduce Mg oxidation, an AlBe5 master alloy was added. Melt homogeneity was ensured by stirring and by removing dissolved gases and non-metallic inclusions. After chemical composition control, the melt was transferred to the holding furnaces through a system of heated launders, where additional treatment, including nitrogen refining, was performed. Immediately before casting, grain refinement was carried out by adding AlTi5B master alloy in the form of rods, while final grain refinement was performed online by continuous addition of AlTi5B wire. The total addition ranged from 2.03 to 2.06 kg/t Al. Prior to entering the mould, the melt was further purified using the ALPUR degassing system and filtered through a ceramic filter. Casting was performed at a melt temperature within the range 715–720 °C, while the main casting parameters, including casting speed, melt level in the moulds, and cooling water flow rate and temperature, were carefully controlled. Two ingots of approximately identical cross-sectional dimensions (520 × 1680 mm) and lengths of 4700–4900 mm were cast from each investigated charge. For the experimental investigation, plates approximately 30 mm thick were cut from the front (F) and rear (R) sections of one ingot per charge and used for subsequent microstructural and mechanical testing.

2.2 Experimental design

In this study, charge was treated as the investigated factor, while slice height (*i*) and slice width (*j*) represented two spatial directions within the ingot cross-section that may be sources of variability in the investigated tensile properties. Figure 1 shows the cross-sections of plates cut from the front and rear sections of an EN AW-5083 alloy ingot with charge 3157. The plates were divided into twelve smaller segments, numbered 1–12 across the cross-section.

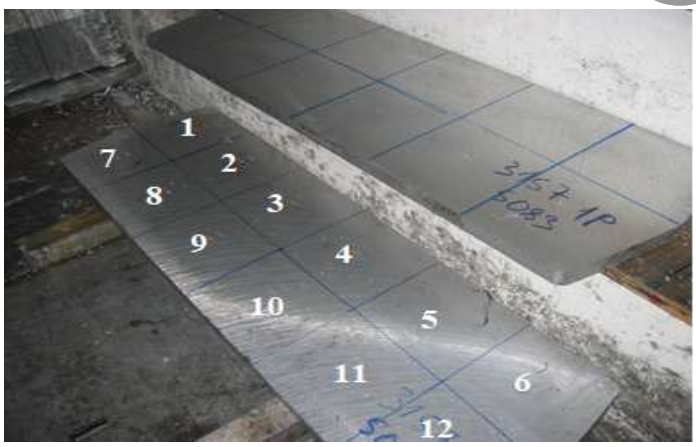

Figure 1. Cross-sections of plates cut from the front and rear sections of the EN AW-5083 alloy ingot (charge 3157), showing the sampling layout consisting of twelve segments (positions 1–12).

Sampling and subsequent analyses were conducted on the lower half of the plates, corresponding to segments 7–12. Only the lower half was considered because, due to the mirror symmetry of the plate cross-section, the cooling and solidification conditions in the upper and lower halves were assumed to be equivalent. For the experimental design, segments 7–12 were treated as six sampling positions across the plate width and labelled j = 1–6. A 6 × 6 Latin square experimental design was used, corresponding to the six investigated charges. In this design, the rows and columns represent two spatial directions within the ingot cross-section, corresponding to the slice height (i) and slice width (j). The casting charges represent the investigated treatments. Each charge appears exactly once in every row and once in every column of the design matrix, allowing the influence of charge on the investigated tensile properties to be evaluated while accounting for spatial variability within the ingot cross-section. Rows in the design matrix correspond to sampling positions along the slice height (i = 1–6), representing the plate thickness, while columns correspond to sampling positions across the slice width (j = 1–6), representing the plate width. Each analysed segment was subdivided along the slice height into six equal sampling positions, corresponding to the rows of the Latin square design. The resulting sampling layout used for tensile testing and microstructural analysis [23] is presented in Table 2. The described Latin square sampling design was applied independently to plates taken from the front (F) and rear (R) sections of the ingots, resulting in two datasets of 36 samples each.

Table 2. Sampling layout according to the Latin square experimental design for all plates taken from the front (F) and rear (R) sections of the six investigated ingots.

Sample Number	Slice height (i)	Slice width (j)	Charge
37F–37R	1	1	3159
38F–38R	1	2	3158
39F–39R	1	3	3157
40F–40R	1	4	3163
41F–41R	1	5	3162
42F–42R	1	6	3160
43F–43R	2	1	3158
44F–44R	2	2	3157
45F–45R	2	3	3163
46F–46R	2	4	3162
47F–47R	2	5	3160
48F–48R	2	6	3159
49F–49R	3	1	3157
50F–50R	3	2	3163
51F–51R	3	3	3162
52F–52R	3	4	3160
53F–53R	3	5	3159
54F–54R	3	6	3158
55F–55R	4	1	3163
56F–56R	4	2	3162
57F–57R	4	3	3160
58F–58R	4	4	3159
59F–59R	4	5	3158
60F–60R	4	6	3157
61F–61R	5	1	3162
62F–62R	5	2	3160
63F–63R	5	3	3159
64F–64R	5	4	3158
65F–65R	5	5	3157
66F–66R	5	6	3163
67F–67R	6	1	3160
68F–68R	6	2	3159
69F–69R	6	3	3158
70F–70R	6	4	3157
71F–71R	6	5	3163
72F–72R	6	6	3162

2.3 Tensile testing

Yield strength ($R_{p0.2}$) and elongation (A_{50}) of EN AW-5083 alloy ingots were determined by tensile testing of samples taken from predefined positions within the ingot cross-section according to the sampling plan. In total, 72 samples were analysed: 36 from the front and 36 from the rear sections of the ingots. Tensile test specimens were prepared in accordance with the standard *ISO 6892-1:2019* [25]. For each sampling position, two parallel tensile tests were performed, and the arithmetic mean of the two measurements was taken as the representative value of the investigated tensile properties. In the following text, these mean values are denoted by $R_{p0.2}$ and A_{50}. The tensile tests were performed using an Amsler universal testing machine (type 10THZ722) with a maximum load capacity of 100 kN. The grain structure was characterised using the semiautomatic mean linear intercept method. The mean linear intercept length ($\bar{l}$) was determined using the intercept procedure on a series of randomly selected microstructural fields. Based on the calculated mean intercept length, the number of grains per unit area (N_A) was determined according to *ASTM E1382* [26]. The reported N_A values represent the arithmetic mean of repeated measurements across multiple microstructural fields, with at least 500 intercept lengths recorded to ensure the statistical reliability of the measurements. The grain structure, expressed as N_A value, and the ultimate tensile strength (*UTS*) for the same samples were reported previously in [23] and were used in the present study to analyse the relationship between microstructural characteristics and the spatial distribution of tensile properties within the ingot cross-section.

2.4 Statistical analysis

Statistical evaluation of the experimental results was conducted using ANOVA based on the applied Latin square experimental design. In this model, the investigated factor was charge, while slice height (*i*) and slice width (*j*) was treated as blocking factors representing spatial positions within the ingot cross-section. The Latin square ANOVA model was used to separate the effect of charge from spatial variability within the ingot. For each investigated tensile property, the analysis of variance included calculation of the sum of squares (*SS*), degrees of freedom (*df*), mean squares (*MS*), F-statistics (*F*), and corresponding p-values (*p*) to evaluate the statistical significance of the analysed sources of variability. Statistical significance was determined using the F-test at the $\alpha = 0.05$ significance level. Parameter estimates represent the deviations of the mean values for individual factor levels from the overall mean value of the investigated property. Additionally, coefficients of variation (*V*) were calculated to assess the dispersion of measured values within each level of the investigated factors. The coefficient of variation was calculated as the ratio of the standard deviation to the corresponding mean, expressed as a percentage. The statistical relationship between the results obtained for the front and rear sections of the ingots was evaluated using the Pearson correlation coefficient (*r*), calculated for paired measurements from corresponding sampling positions. All statistical calculations were performed using StatSoft STATISTICA 13 (Experimental Design) and the R statistical environment (version 4.4.3).

3 Results and discussion

3.1 Tensile properties of the ingots

Tables 3 and 4 present the measured values of yield strength ($R_{p0.2}$), elongation (A_{50}) and the corresponding values of the number of grains per unit area (N_A) [23] for samples taken from the front (F) and rear (R) sections of the investigated ingots. For the front sections of the ingots, the measured yield strength ranges from 171.5 MPa to 213.5 MPa, while elongation ranges from 17% to 25%. In the rear sections, yield strength ranges from 172.0 MPa to 221.0 MPa, and elongation varies from 14 % to 27 %.

Table 3. Yield strength ($R_{p_{0.2}}$), elongation (A_{50}) and number of grains per unit area (N_A) [23] measured at predefined sampling locations in the front (F) section of the investigated EN AW-5083 alloy ingots.

Sample Number	$R_{p_{0.2}}$, MPa	A_{50}, %	N_A, No./mm^2
37F	188.0	21.0	88.11
38F	188.0	22.0	88.79
39F	182.0	17.0	80.76
40F	183.5	17.0	78.89
41F	199.5	19.0	83.87
42F	188.0	25.0	85.71
43F	178.5	21.5	105.97
44F	178.5	18.0	67.89
45F	185.0	17.0	59.76
46F	183.5	17.0	80.08
47F	201.0	20.5	84.77
48F	212.5	21.0	86.22
49F	176.0	21.0	102.80
50F	190.0	19.0	72.81
51F	182.0	19.0	87.49
52F	202.0	23.0	68.56
53F	213.5	20.0	89.75
54F	203.0	22.0	101.53
55F	203.0	23.0	92.59
56F	196.0	22.0	118.80
57F	171.5	22.0	113.63
58F	207.5	22.0	97.43
59F	210.5	23.0	83.27
60F	194.5	22.0	93.79
61F	208.5	21.0	119.36
62F	198.5	25.0	115.89
63F	192.5	22.0	93.24
64F	172.0	24.0	131.08
65F	201.0	23.0	133.71
66F	181.5	21.0	86.03
67F	182.5	23.0	137.55
68F	188.0	23.0	154.69
69F	184.0	22.0	137.31
70F	189.5	22.0	154.82
71F	201.0	22.5	126.71
72F	190.0	23.0	117.17

Table 4. Yield strength ($R_{p_{0.2}}$), elongation (A_{50}) and number of grains per unit area (N_A) measured at predefined sampling locations in the rear (R) section of the investigated EN AW-5083 alloy ingots.

Sample Number	$R_{p_{0.2}}$, MPa	A_{50}, %	N_A, No./mm^2
37R	196.0	18.0	115.68
38R	173.0	17.0	60.70
39R	180.5	16.0	61.08
40R	191.5	15.0	52.22
41R	213.5	21.0	69.73
42R	210.0	21.5	101.08
43R	174.0	21.0	118.89
44R	181.0	14.0	67.92
45R	190.0	15.0	50.44
46R	184.0	19.0	74.60
47R	196.0	17.5	81.89
48R	203.0	18.0	122.10
49R	184.0	21.0	122.00
50R	175.5	19.0	63.74
51R	188.5	18.0	87.12
52R	192.0	19.0	73.88
53R	206.0	17.5	86.51
54R	214.0	24.0	85.41
55R	211.0	21.0	73.73
56R	188.5	21.0	86.82
57R	199.5	21.0	108.32
58R	189.0	20.0	95.88
59R	195.5	25.5	83.31
60R	198.5	26.0	87.39
61R	196.0	23.0	119.86
62R	196.0	23.0	121.35
63R	172.0	24.0	133.75
64R	221.0	21.5	103.75
65R	189.0	25.0	118.35
66R	202.0	27.0	108.34
67R	173.5	24.0	155.99
68R	202.0	23.0	168.65
69R	182.5	22.0	157.89
70R	215.5	25.0	132.49
71R	208.5	24.5	122.97
72R	207.5	24.5	144.74

Comparison of the results presented in Tables 3 and 4 indicates that the investigated EN AW-5083 alloy ingots exhibit spatial variations in tensile properties across the ingot cross-section. However, the overall ranges of yield strength and elongation remain similar for the front and rear sections of the ingots. Variations among individual sampling locations indicate that tensile properties are not uniform across the ingot cross-section. As shown in Tables 3 and 4, the number of grains per unit area varies considerably between the analysed positions, indicating corresponding variations in the microstructure. Such spatial variations are characteristic of DC-cast aluminium alloys, in which non-uniform heat extraction and solidification conditions across the ingot cross-section lead to local differences in microstructure, segregation behaviour, and consequently mechanical properties [9]. In industrial DC casting, higher cooling rates near the ingot surface and lower cooling rates in

the central regions promote spatial variations in grain structure and solute distribution, which may contribute to differences in the local tensile properties [10], [15].

The relatively narrow range of yield strength values indicates that the investigated ingots maintain a generally stable strength level across the analysed sampling positions. In contrast, the greater scatter observed in elongation values suggests that elongation (A_{50}) is more sensitive to local microstructural variations within the ingot cross-section, such as variations in grain size reflected by differences in the number of grains per unit area, as well as other microstructural characteristics associated with local solidification conditions. The overall mean yield strength of samples taken from the front section of the ingots is 191.85 MPa, while that for the rear section is 194.44 MPa, indicating very similar average strength levels along the ingot length. This behaviour is consistent with the strengthening mechanisms typical of Al–Mg alloys, in which yield strength is predominantly controlled by solid-solution strengthening associated with the Mg content rather than by local variations in grain structure [1]. The number of grains per unit area (N_A) is inversely related to the average grain size and therefore reflects the degree of grain refinement in the microstructure. According to the Hall–Petch relationship, a finer grain structure (higher N_A) generally increases yield strength due to the strengthening effect of grain boundaries, and may also improve ductility through more uniform plastic deformation [6], [7].

The observed relationship between the tensile properties and the parameter N_A further suggests that local differences in grain structure may contribute to the measured variations in tensile behaviour. In this context, the strengthening effect associated with grain refinement may partly explain the local differences in tensile response. Similar effects of grain refinement on the mechanical behaviour of Al–Mg alloys have been reported previously [28]. Comparable relationships between grain structure development and mechanical properties in DC-cast aluminium alloys have also been reported [29]. Earlier investigations on the same alloy system showed that higher values of the parameter N_A are associated with increased tensile strength in the as-cast condition [23]. Taken together with the present results, this observation indicates that local variations in grain size that develop during solidification may influence the spatial distribution of tensile properties in DC-cast EN AW-5083 alloy ingots. To assess the statistical significance of the observed spatial variations in tensile properties, an analysis of variance (ANOVA) was performed. The results of this analysis are presented in the following section.

3.2 Influence of spatial variables on yield strength

Tables 5 and 6 present the mean values of yield strength together with the corresponding parameter estimates (expressed as deviations from the overall mean), standard deviations and coefficients of variation obtained from the Latin square experimental design. The results are given for the front ($R_{p0.2}(F)$) and rear ($R_{p0.2}(R)$) sections of the ingots. In the front section of the ingots (Table 5), the mean $R_{p0.2}(F)$ values for the analysed charges range from 186.92 MPa to 200.33 MPa. Along the slice height, the mean values range from 188.17 MPa to 197.17 MPa, while across the slice width they range from 182.83 MPa to 204.42 MPa. In the rear section of the ingots (Table 6), the mean $R_{p0.2}(R)$ values range from 191.42 MPa to 196.42 MPa depending on the charge. Along the slice height, the values range from 188.00 MPa to 198.25 MPa, while across the slice width they range from 185.50 MPa to 205.83 MPa.

Table 5. Mean yield strength ($R_{p_{0.2}}$(F)), parameter estimates, standard deviations and coefficients of variation ($V_{Rp0.2}$(F)) for the ingot front section.

Variables	Level	$R_{p_{0.2}}$(F), MPa	Parameter Estimate	Standard deviation	$V_{Rp0.2}$(F), %
Charge	3157	186.92	-4.93	9.76	5.22
	3158	189.33	-2.51	14.72	7.77
	3159	200.33	8.49	12.15	6.07
	3160	190.58	-1.26	12.15	6.37
	3162	193.25	1.40	10.11	5.23
	3163	190.67	-1.18	9.24	4.85
Slice height (*i*)	1	188.17	-3.68	6.14	3.26
	2	189.83	-2.01	13.85	7.29
	3	194.41	2.57	14.20	7.30
	4	197.17	5.32	14.04	7.12
	5	192.33	0.49	13.46	7.00
	6	189.17	-2.68	6.53	3.45
Slice width (*j*)	1	189.42	-2.43	13.40	7.07
	2	189.83	-2.01	7.05	3.71
	3	182.83	-9.01	6.77	3.70
	4	189.68	-2.18	13.10	6.91
	5	204.42	12.57	5.98	2.92
	6	194.92	3.07	11.20	5.74

Table 6. Mean yield strength ($R_{p_{0.2}}$(R)), parameter estimates, standard deviations and coefficients of variation ($V_{Rp0.2}$(R)) for the ingot rear section.

Variables	Level	$R_{p_{0.2}}$(R), MPa	Parameter Estimate	Standard deviation	$V_{Rp0.2}$(R), %
Charge	3157	191.42	-3.03	13.56	7.08
	3158	193.33	-1.11	20.50	10.60
	3159	194.67	0.22	12.64	6.50
	3160	194.50	0.06	11.97	6.16
	3162	196.33	1.89	11.78	6.00
	3163	196.42	1.97	13.36	6.80
Slice height (*i*)	1	194.08	-0.36	15.94	8.21
	2	188.00	-6.44	10.53	5.60
	3	193.33	-1.11	14.27	7.38
	4	197.00	2.56	8.28	4.20
	5	196.00	1.56	16.04	8.18
	6	198.25	3.81	16.51	8.33
Slice width (*j*)	1	189.08	-5.36	14.64	7.74
	2	186.00	-8.44	11.55	6.21
	3	185.50	-8.94	9.40	5.07
	4	198.83	4.39	15.40	7.75
	5	201.42	6.97	9.33	4.63
	6	205.83	11.39	5.72	2.78

Figure 2 shows the graphical representation of the influence of the analysed variables on mean yield strength ($R_{p_{0.2}}$) for the front and rear sections of the ingots.

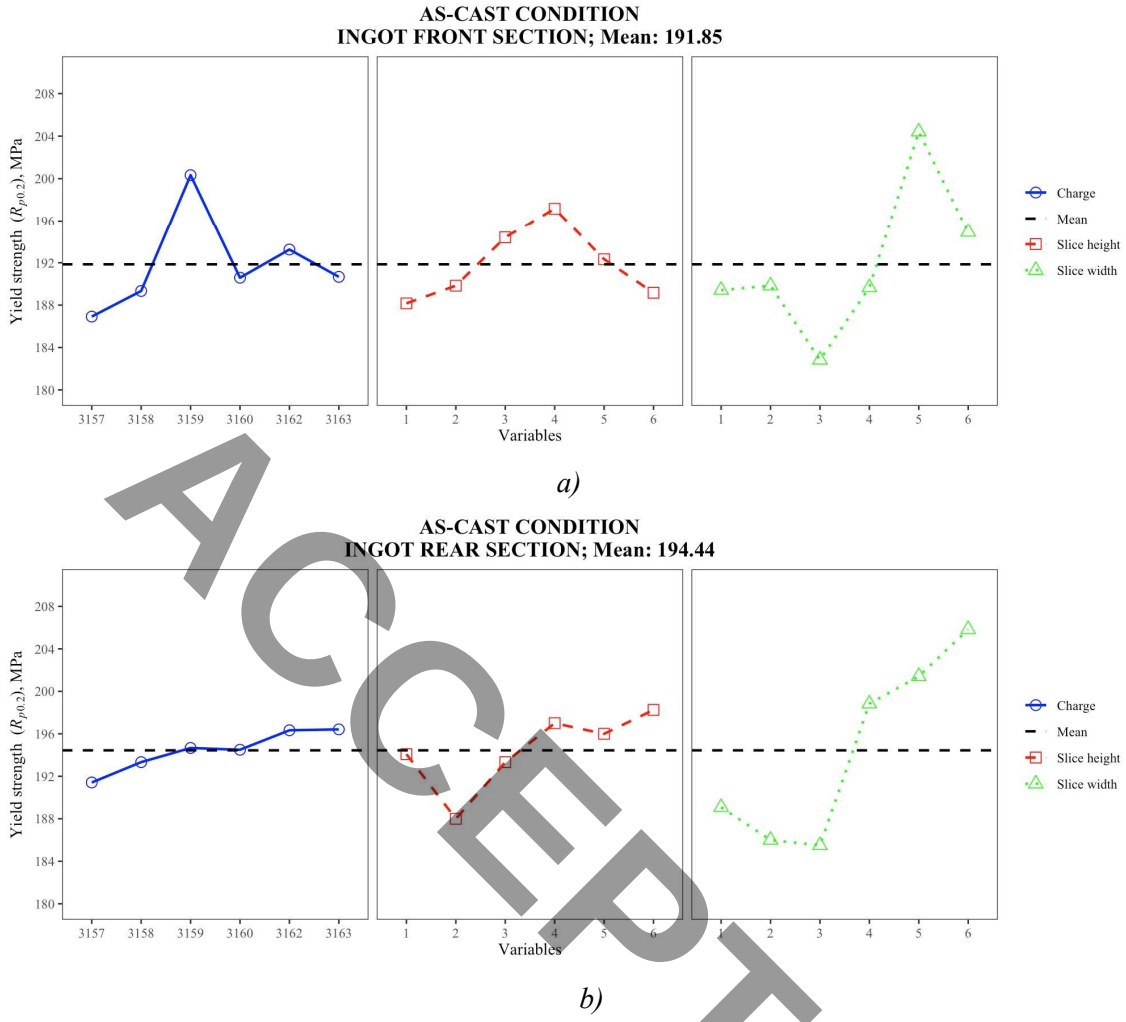

Figure 2. Graphical representation of the influence of individual variables on $R_{p0.2}$: a) ingot front section (F); b) ingot rear section (R).

As shown in Figure 2, the mean $R_{p0.2}$ values for the front and rear sections of the ingots fluctuate around their respective mean values without a clear spatial trend across the ingot cross-section. This behaviour is typical for aluminium alloys produced by the DC casting process, where local variations in cooling conditions and thermal gradients during solidification may lead to spatial differences in microstructure and chemical segregation within the ingot [9], [15]. However, the relatively small deviations observed in this study indicate that these local variations have only a moderate effect on the yield strength of the alloy under investigation. To evaluate the statistical significance of the observed variations, analysis of variance (ANOVA) was performed according to the applied Latin square experimental design. The ANOVA results for yield strength $R_{p0.2}$ are presented in Tables 7 and 8.

Table 7. ANOVA results for yield strength ($R_{p0.2}$) in the ingot front section.

Variable	SS	df	MS	F	p
Charge	645.62	5	129.12	1.27	0.315
Slice height (*i*)	359.54	5	71.91	0.71	0.625
Slice width (*j*)	1580.29	5	316.06	3.11	0.031
Residual	2033.97	20	101.70		

In the front section of the ingots (Table 7), slice width has a statistically significant effect on $R_{p0.2}$ ($p = 0.031$), whereas the effects of charge ($p = 0.315$) and slice height ($p = 0.625$) are not statistically significant.

Table 8. ANOVA results for yield strength ($R_{p0.2}$) in the ingot rear section.

Variable	SS	df	MS	F	p
Charge	107.47	5	21.49	0.12	0.985
Slice height (*i*)	397.97	5	79.59	0.46	0.801
Slice width (*j*)	2265.81	5	453.16	2.62	0.056
Residual	3460.14	20	173.01		

In the rear section of the ingots (Table 8), none of the analysed variables has a statistically significant effect on $R_{p0.2}$. However, the effect of slice width (p = 0.056) is close to the significance threshold. The ANOVA results indicate that slice width has the strongest effect on $R_{p0.2}$ among the analysed spatial variables, particularly in the front section of the ingots. This behaviour can be related to the solidification conditions in DC-cast ingots, where the distance from the mould walls and the local cooling intensity vary across the ingot width. These variations may lead to differences in microstructure and segregation patterns across the ingot cross-section [9], [15]. The relationship between the yield strength values obtained for the front and rear sections of the ingots was further analysed using Pearson correlation analysis. The Pearson correlation coefficients $r(R_{p0.2})$ between the front and rear sections of the ingots for each charge are presented in Table 9.

Table 9. Pearson correlation coefficients $r(R_{p0.2})$ between the front and rear sections of the investigated ingots for each charge.

Charge	3157	3158	3159	3160	3162	3163
$r(R_{p0.2})$	0.55	0.09	0.37	0.05	0.01	0.30

The correlation coefficients range from 0.01 to 0.55, indicating relatively weak correlations between the front and rear sections of the ingots. This suggests that local variations in yield strength within the ingot cross-section are not strongly correlated along the ingot length. This behaviour may be related to local differences in microstructure formed during solidification, particularly variations in grain structure associated with local cooling conditions typical of DC-cast Al–Mg alloys [1], [16], [27].

3.3 Influence of spatial variables on elongation

Tables 10 and 11 present the mean values of elongation together with the corresponding parameter estimates, standard deviations and coefficients of variation obtained from the Latin square experimental design for elongation (A_{50}) in the front and rear sections of the investigated EN AW-5083 alloy ingots, denoted as $A_{50(F)}$ and $A_{50(R)}$, respectively.

Table 10. Mean elongation ($A_{50}(F)$), parameter estimates, standard deviations and coefficients of variation ($V_{A50}(F)$) for the ingot front section.

Variables	Level	$A_{50}(F)$	Parameter Estimate	Standard deviation	$V_{A50}(F)$, %
Charge	3157	20.50	-0.76	2.43	11.85
	3158	22.42	1.15	0.92	4.09
	3159	21.50	0.24	1.05	4.88
	3160	23.08	1.82	1.74	7.56
	3162	20.17	-1.10	2.23	11.05
	3163	19.92	-1.35	2.65	13.32
Slice height (*i*)	1	20.17	-1.10	3.13	15.50
	2	19.17	-2.10	2.07	10.78
	3	20.67	-0.60	1.63	7.90
	4	22.33	1.07	0.52	2.31
	5	22.67	1.40	1.63	7.20
	6	22.58	1.32	0.49	2.18
Slice width (*j*)	1	21.75	0.49	0.99	4.54
	2	21.50	0.24	2.59	12.04
	3	19.83	-1.43	2.48	12.52
	4	20.83	-0.43	3.06	14.69
	5	21.33	0.07	1.72	8.07
	6	22.33	1.07	1.51	6.74

Table 11. Mean elongation ($A_{50}(R)$), parameter estimates, standard deviations and coefficients of variation ($V_{A50}(R)$) for the ingot rear section.

Variables	Level	$A_{50}(R)$	Parameter Estimate	Standard deviation	$V_{A50}(R)$, %
Charge	3157	21.17	0.26	5.12	24.17
	3158	21.83	0.93	2.91	13.33
	3159	20.08	-0.82	2.80	13.94
	3160	21.00	0.10	2.43	11.57
	3162	21.08	0.18	2.42	11.46
	3163	20.25	-0.65	4.92	24.28
Slice height (*i*)	1	18.08	-2.82	2.65	14.67
	2	17.42	-3.49	2.58	14.80
	3	19.75	-1.15	2.40	12.17
	4	22.42	1.51	2.62	11.67
	5	23.92	3.01	1.91	7.98
	6	23.83	2.93	1.13	4.72
Slice width (*j*)	1	21.33	0.43	2.07	9.68
	2	19.50	-1.40	3.56	18.28
	3	19.33	-1.57	3.56	18.41
	4	19.92	-0.99	3.29	16.53
	5	21.83	0.93	3.71	16.99
	6	23.50	2.60	3.29	13.98

In the front section of the ingots (Table 10), the mean $A_{50}(F)$ values for the analysed charges range from 19.92 % to 23.08 %. Along the slice height, the mean elongation values range from 19.17 % to 22.67 %, while across the slice width they range from 19.83 % to 22.33 %. In the rear section of the ingots (Table 11), the mean $A_{50}(R)$ values range from 20.08 % to 21.83 % depending on the charge. Along the slice height, the mean elongation values range from 17.42 % to 23.92 %, while across the slice width they range from 19.33 % to 23.50 %. Figure 3 shows the graphical representation of the influence of the analysed variables on mean elongation (A_{50}) for the front and rear sections of the ingots.

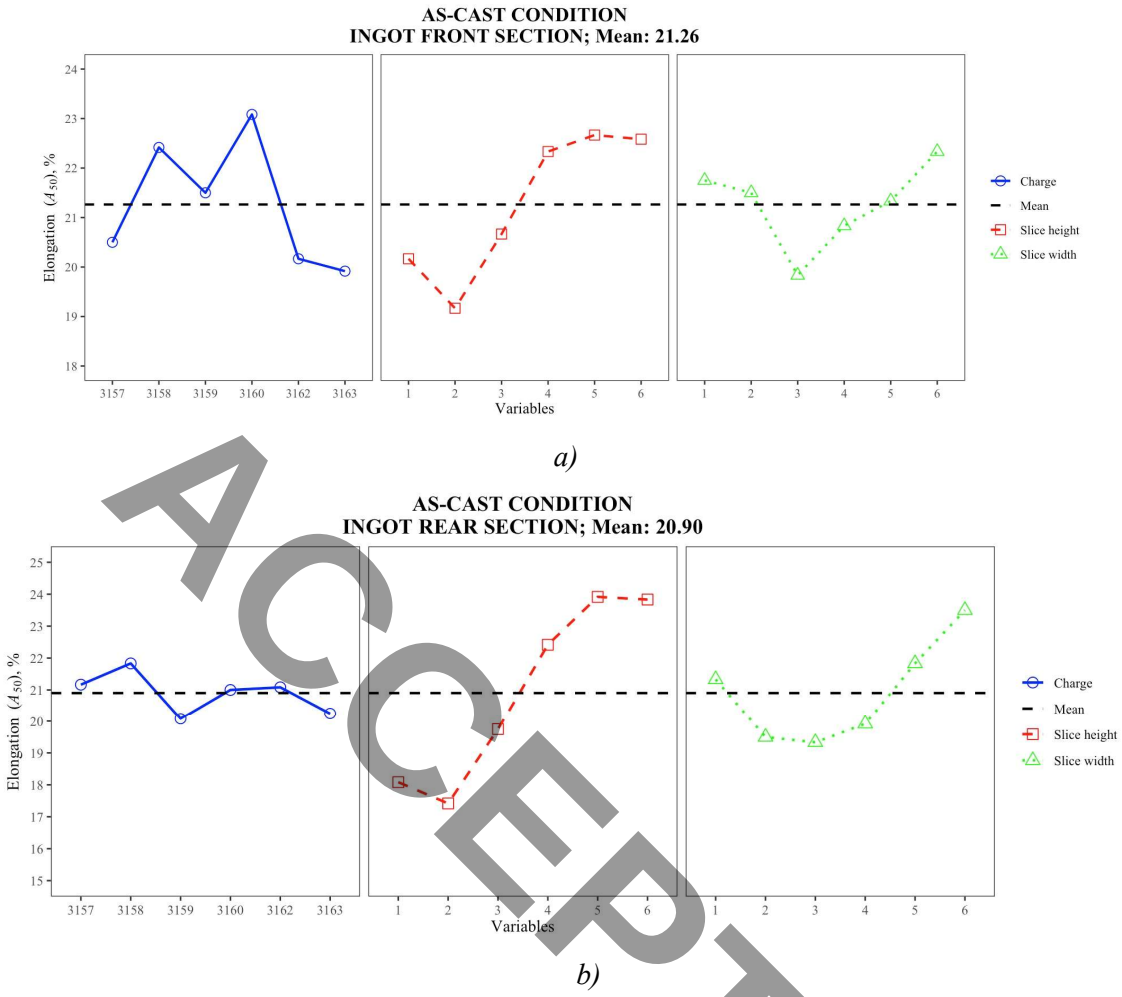

Figure 3. Graphical representation of the influence of individual variables on elongation A_{50}: a) ingot front section; b) ingot rear section.

As shown in Figure 3, elongation (A_{50}) exhibits a clear spatial trend across the ingot cross-section. The effect of slice height shows the most pronounced systematic variation, with parameter estimates increasing from −2.10 % at level i = 2 to +1.40 % at level i = 5 in the front section of the ingots, indicating higher elongation towards the ingot edges. A similar trend is observed in the rear section, where parameter estimates range from −3.49% at level i = 2 to +3.01% at level i = 5. Variations associated with slice width are less pronounced but still indicate slightly higher elongation values near the ingot edges. In contrast, the effect of charge produces only moderate deviations around the overall mean elongation values of $A_{50}(F)$ = 21.26 % and $A_{50}(R)$ = 20.90 %. These results indicate that spatial position within the ingot cross-section has a stronger influence on elongation than differences between individual casting charges. The mean elongation values for the front and rear sections of the ingots remain very similar, indicating comparable average ductility levels along the ingot length. To evaluate the statistical significance of the observed variations, analysis of variance (ANOVA) was performed according to the applied Latin square experimental design. The results of this analysis are presented in Tables 12 and 13.

Table 12. ANOVA results for elongation (A_{50}) in the ingot front section.

Variable	SS	df	MS	F	p
Charge	49.78	5	9.96	7.23	0.001
Slice height (i)	64.87	5	12.97	9.42	<0.001
Slice width (j)	22.03	5	4.41	3.20	0.028
Residual	27.56	20	1.38		

In the front section of the ingots (Table 12), all analysed variables show statistically significant effects on elongation: charge ($p = 0.001$), slice height ($p < 0.001$) and slice width ($p = 0.028$). Among these variables, slice height has the strongest influence on elongation.

Table 13. ANOVA results for elongation (A_{50}) in the ingot rear section.

Variable	SS	df	MS	F	p
Charge	12.45	5	2.49	0.77	0.580
Slice height (*i*)	248.37	5	49.67	15.43	<0.001
Slice width (*j*)	79.20	5	15.84	4.92	0.004
Residual	64.39	20	3.22		

In the rear section of the ingots (Table 13), slice height ($p < 0.001$) and slice width ($p = 0.004$) have statistically significant effects on elongation A_{50}, whereas the effect of charge ($p = 0.580$) is not statistically significant. The relationship between elongation values obtained for the front and rear sections of the ingots was further analysed using Pearson correlation analysis. The Pearson correlation coefficients $r(A_{50})$ between the front and rear sections of the ingots for each charge are presented in Table 14.

Table 14. Pearson correlation coefficients $r(A_{50})$ between the front and rear sections of the investigated ingots for each charge.

Charge	3157	3158	3159	3160	3162	3163
$r(A_{50})$	0.94	0.26	0.83	0.67	0.79	0.80

The correlation coefficients range from 0.26 to 0.94, indicating correlations ranging from weak to very strong depending on the individual charge. In most cases, the correlations are moderate to strong, suggesting that the spatial distribution of elongation is largely preserved along the ingot length. The dominant influence of slice height on elongation can be related to the solidification conditions in DC-cast ingots. During DC casting, non-uniform heat extraction across the ingot cross-section leads to differences in local cooling rates and microstructure development [9], [15]. Earlier investigations of the same alloy system showed that higher values of the microstructural parameter NA were observed near the ingot edges [23], corresponding to a finer grain structure, which is generally associated with improved ductility. Higher cooling rates near the ingot surface promote grain refinement and contribute to the development of such microstructures during solidification, which may contribute to increased elongation values in the edge regions of the ingot. In contrast, the coarser grain structure typically present in the central region may result in lower elongation values and greater scatter in the measured results [9], [27]. A comparison of the results obtained for yield strength ($R_{p0.2}$) and elongation (A_{50}) further highlights the different sensitivity of these properties to microstructural heterogeneity. While the spatial variability of yield strength is relatively limited and most sources of variability are statistically insignificant, elongation exhibits a markedly stronger dependence on spatial position within the ingot cross-section.

4 Conclusion

This study analysed the spatial distribution of tensile properties in EN AW-5083 aluminium alloy ingots produced under industrial conditions using the semi-continuous Direct Chill casting process. The results show that both yield strength and elongation vary across the ingot cross-section. Yield strength values ranged from 171.5 MPa to 221.0 MPa, while elongation varied from 14 % to 27 %. Despite these local variations, the average values of the investigated properties were very similar for the front and rear sections of the ingots, indicating relatively uniform mechanical behaviour along the casting direction. Statistical analysis confirmed that spatial position within the ingot cross-section has a more consistent influence on the investigated tensile properties, particularly on elongation, than differences between individual charges. In particular, slice width had a statistically significant effect on yield strength in the front section of the ingots, while both slice height and slice width significantly affected elongation. These results indicate a pronounced centre–edge effect typical of DC-cast aluminium ingots, where higher cooling rates near the mould walls promote finer grain structures and improved plastic deformation capability compared with the more slowly solidified central

regions. The results further demonstrate that the investigated tensile properties exhibit different sensitivities to spatial microstructural variations within the ingot cross-section. While yield strength showed relatively limited spatial variability, elongation exhibited considerably greater sensitivity to local solidification conditions. This behaviour is consistent with the spatial distribution of the microstructural parameter, expressed as the number of grains per unit area, suggesting that grain-structure development during solidification plays an important role in controlling the alloy's tensile response. Overall, the investigated EN AW-5083 alloy ingots produced under the applied industrial casting conditions exhibit a satisfactory level of structural and mechanical homogeneity along the ingot length.

The remaining variations across the ingot cross-section are primarily attributable to local microstructural differences that develop during solidification in the DC casting process. From an industrial perspective, the results indicate that the applied casting technology provides sufficiently stable solidification conditions to ensure relatively uniform tensile properties in the investigated EN AW-5083 ingots. The presented approach contributes to a better understanding of the relationship between solidification conditions, microstructure, and tensile behaviour, and may support further optimisation of process parameters in industrial Direct Chill casting of aluminium alloys.

Acknowledgement

The investigation was carried out as part of the Institutional Research Project the "Design and characterisation of innovative engineering alloys/products (KIIL)" financed by the EU – Next Generation EU. The views and opinions expressed are those of the author and do not necessarily reflect the official positions of the European Union or the European Commission. Neither the European Union nor the European Commission can be held responsible for them. The investigation was performed on equipment within the infrastructural scientific projects: Center for Founding - SIMET (Code: KK.01.1.1.02.0020); and the VIRTULAB - Integrated Laboratory for Primary and Secondary Raw Materials (Code: KK.01.1.1.02.0022).

References

[1] C.-R. Song, B.-X. Dong, S.-Y. Zhang, H.-Y. Yang, L. Liu, J. Kang, J. Meng, C.-J. Luo, C.-G. Wang, K. Cao, J. Qiao, S.-L. Shu, M. Zhu, F. Qiu, and Q.-C. Jiang, "Recent progress of Al–Mg alloys: Forming and preparation process, microstructure manipulation and application," *J. Mater. Res. Technol.*, vol. 31, pp. 3255–3286, 2024, doi: 10.1016/j.jmrt.2024.07.051.

[2] J. Thavamani, N. Vadivelan, V. Rajasekar, and P. V. Jeyakarthikeyan, "Study of thermal and mechanical properties in Al–Mg alloys for lightweight thermal applications," *Int. Res. J. Adv. Eng. Hub*, vol. 3, no. 6, pp. 2727–2737, 2025, doi: 10.47392/IRJAEH.2025.0405.

[3] J. Hirsch and T. Al-Samman, "Superior light metals by texture engineering: Optimized aluminum and magnesium alloys for automotive applications," *Acta Materialia*, vol. 61, no. 3, pp. 818–843, 2013, doi: 10.1016/j.actamat.2012.10.044.

[4] S. Toros, F. Ozturk, and I. Kacar, "Review of warm forming of aluminum–magnesium alloys," *J. Mater. Process. Technol.*, vol. 207, no. 1–3, pp. 1–12, 2008, doi: 10.1016/j.jmatprotec.2008.03.057.

[5] D. Istrate, B.-G. Sbârcea, A. M. Demian, A. D. Buzatu, L. Salcianu, I. Bordeasu, L. M. Micu, C. Ghera, B. Florea, and B. Ghiban, "Correlation between mechanical properties, structural characteristics and cavitation resistance of cast aluminum alloy type 5083," *Crystals*, vol. 12, no. 11, Art. no. 1538, 2022, doi: 10.3390/cryst12111538.

[6] M. S. Haque, S. M. N. Rokon, and M. S. Kaiser, "Strengthening and softening behavior of non-heat-treatable aluminum alloys subject to deformation and annealing treatment," *Mater. Today Proc.*, vol. 82, pp. 151–157, 2023, doi: 10.1016/j.matpr.2022.12.113.

[7] J. R. Davis, Aluminum and Aluminum Alloys. Materials Park, OH, USA: ASM International, 1993.

[8] O. Engler and J. Hirsch, "Texture control by thermomechanical processing of AA6xxx Al–Mg–Si sheet alloys for automotive applications—a review," *Mater. Sci. Eng. A*, vol. 336, no. 1–2, pp. 249–262, 2002, doi: 10.1016/S0921-5093(01)01968-2.

[9] R. Nadella, D. G. Eskin, Q. Du, and L. Katgerman, "Macrosegregation in direct-chill casting of aluminium alloys," *Prog. Mater. Sci.*, vol. 53, no. 3, pp. 421–480, 2008, doi: 10.1016/j.pmatsci.2007.10.001.

[10] D. G. Eskin and L. Katgerman, "A quest for increased productivity of the DC casting process," *Metall. Mater. Trans. A*, vol. 38, no. 7, pp. 1511–1518, 2007, doi: 10.1007/s11661-007-9177-5.
[11] K. Rajagukguk, S. Suyitno, H. Saptoadi, I. Kusumaningtyas, B. Arifvianto, and M. Mahardika, "Remelting of aluminum scrap into billets using direct chill casting," *Arch. Foundry Eng.*, vol. 24, no. 1, pp. 40–49, 2024, doi: 10.24425/afe.2024.149250.
[12] J. C. Méndez, R. R. Ambriz, D. Jaramillo, and G. Plascencia, "Depicting aluminium DC casting by means of dimensionless numbers," in *Advanced Casting Technologies*. London, U.K.: IntechOpen, 2017, doi: 10.5772/intechopen.71893.
[13] Y. Zhang, X. Liu, Q. Zhu, Y. Zuo, R. Wang, and H. Jiang, "Understanding of macro-segregation in direct-chill cast 2024 alloy with intensive melt shearing based on the evolution of microstructure and temperature field," *J. Mater. Res. Technol.*, vol. 27, pp. 7257–7272, 2023, doi: 10.1016/j.jmrt.2023.11.224.
[14] M. Jolly and L. Katgerman, "Modelling of defects in aluminium cast products," *Prog. Mater. Sci.*, vol. 123, Art. no. 100824, 2022, doi: 10.1016/j.pmatsci.2021.100824.
[15] D. G. Eskin, *Physical Metallurgy of Direct Chill Casting of Aluminum Alloys*. Boca Raton, FL, USA: CRC Press, 2008, doi: 10.1201/9781420062823.
[16] N. Jamaly, N. Haghdadi, and A. B. Phillion, "Microstructure, macrosegregation, and thermal analysis of direct chill cast AA5182 aluminum alloy," *J. Mater. Eng. Perform.*, vol. 24, no. 5, pp. 2067–2073, 2015, doi: 10.1007/s11665-015-1480-7.
[17] M. A. Easton and D. H. StJohn, "Grain refinement of aluminum alloys: Part I. The nucleant and solute paradigms—a review of the literature," *Metall. Mater. Trans. A*, vol. 30, pp. 1613–1623, 1999, doi: 10.1007/s11661-999-0098-5.
[18] D. H. StJohn, M. A. Easton, M. Qian, and J. Taylor, "Grain refinement of aluminium alloys," *Metall. Mater. Trans. A*, vol. 44, pp. 2935–2949, 2013, doi: 10.1007/s11661-013-1798-7.
[19] A. L. Greer, A. M. Bunn, A. Tronche, P. V. Evans, and D. J. Bristow, "Modelling of inoculation of metallic melts: application to grain refinement of aluminium by Al–Ti–B," *Acta Materialia*, vol. 48, no. 11, pp. 2823–2835, 2000, doi: 10.1016/S1359-6454(00)00094-X.
[20] D. G. Eskin and L. Katgerman, "Solidification phenomena related to direct chill casting of aluminium alloys: Fundamental studies and future challenges," *Mater. Technol.*, vol. 24, no. 3, pp. 152–156, 2009, doi: 10.1179/106678509X12489478523537.
[21] N. Dolić and Z. Zovko Brodarac, "Evaluation of EN AW-5083 aluminum alloy homogeneity using statistical analysis of mechanical properties," *J. Min. Metall., Sect. B*, vol. 53, no. 3, pp. 429–439, 2017, doi: 10.2298/JMMB170812046D**.**
[22] N. Dolić, A. Markotić, and F. Unkić, "Structural homogeneity of direct-chill cast ingots of aluminum alloy EN AW-5083," *Metall. Mater. Trans. B*, vol. 38, no. 3, pp. 491–495, 2007, doi: 10.1007/s11663-006-9008-z.
[23] N. Dolić, I. Bunjan, and F. Kozina, "Correlation of mechanical and microstructural properties in as-cast condition of EN AW-5083 aluminum alloy using statistical analysis," in Proc. of the 18th International Foundrymen Conference – Coexistence of Material Science and Sustainable Technology in Economic Growth, Sisak, Croatia, May 15–17, 2019.
[24] *Aluminium and aluminium alloys—Chemical composition and form of wrought products—Part 3: Chemical composition*, EN 573-3:2009. Brussels, Belgium: European Committee for Standardization, 2009.
[25] *Metallic materials—Tensile testing—Part 1: Method of test at room temperature*, ISO 6892-1:2019. Geneva, Switzerland: International Organization for Standardization, 2019.
[26] *Standard test methods for determining average grain size using semiautomatic and automatic image analysis*, ASTM E1382-97. West Conshohocken, PA, USA: ASTM International, 1997.
[27] T. Radetić, M. Popović, and E. Romhanji, "Microstructure evolution of a modified AA5083 aluminum alloy during a multistage homogenization treatment," *Mater. Charact.*, vol. 65, pp. 16–27, 2012, doi: 10.1016/j.matchar.2011.12.006.
[28] A. A. Alghannam, M. S. Soliman, A. H. Seikh, I. A. Alnaser, A. Fouly, J. A. Mohammed, S. A. Ragab, and H. S. Abdo, "Investigation on mechanical properties and corrosion resistance of Ti-modified AA5083 aluminum alloy for aerospace and automotive applications," *Sci. Rep.*, vol. 13, Art. no. 11535, 2023, doi: 10.1038/s41598-023-38510-1.

[29] A. M. Glenn, S. P. Russo, and P. J. K. Paterson, "The effect of grain refining on macrosegregation and dendrite arm spacing of direct chill cast AA5182," *Metall. Mater. Trans. A*, vol. 34, no. 7, pp. 1513–1523, 2003, doi: 10.1007/s11661-003-0263-1.